

Optical-model potential for electron and positron elastic scattering by atoms

Francesc Salvat*

Facultat de Física (ECM), Universitat de Barcelona, Societat Catalana de Física (IEC), Diagonal 647, 08028 Barcelona, Spain

(Received 30 March 2003; published 14 July 2003)

An optical-model potential for systematic calculations of elastic scattering of electrons and positrons by atoms and positive ions is proposed. The electrostatic interaction is determined from the Dirac-Hartree-Fock self-consistent atomic electron density. In the case of electron projectiles, the exchange interaction is described by means of the local-approximation of Furness and McCarthy. The correlation-polarization potential is obtained by combining the correlation potential derived from the local density approximation with a long-range polarization interaction, which is represented by means of a Buckingham potential with an empirical energy-dependent cutoff parameter. The absorption potential is obtained from the local-density approximation, using the Born-Ochkur approximation and the Lindhard dielectric function to describe the binary collisions with a free-electron gas. The strength of the absorption potential is adjusted by means of an empirical parameter, which has been determined by fitting available absolute elastic differential cross-section data for noble gases and mercury. The Dirac partial-wave analysis with this optical-model potential provides a realistic description of elastic scattering of electrons and positrons with energies in the range from ~ 100 eV up to ~ 5 keV. At higher energies, correlation-polarization and absorption corrections are small and the usual static-exchange approximation is sufficiently accurate for most practical purposes.

DOI: 10.1103/PhysRevA.68.012708

PACS number(s): 34.80.Bm, 34.85.+x

I. INTRODUCTION

Elastic scattering has a prominent effect on the transport of fast electrons and positrons through matter. Owing to the smallness of the electron mass m_e , these particles may undergo relatively large angular deflections in single-interaction events and, as a consequence, their trajectories are tortuous. Knowledge of accurate differential cross sections (DCS) for elastic scattering of electrons and positrons is necessary for studies of electron and positron transport in matter, which are needed for many practical applications. These include quantitative analysis in surface electron and positron spectroscopies, detector design and characterization, radiation dosimetry, and radiotherapy treatment planning. Electron-transport calculations are frequently performed by means of Monte Carlo simulation (see, e.g., Refs. [1,2]), which requires systematic tabulations of elastic DCSs as functions of the projectile kinetic energy E and the scattering angle θ .

For projectiles with kinetic energy larger than, say, ~ 5 keV, elastic collisions can be described by means of the static-field approximation, in which the target atom is considered as a frozen charge distribution and the interaction with the projectile is assumed to reduce to the electrostatic interaction (see, e.g., Ref. [3]). In the case of projectile electrons, an approximate local exchange potential [4] may be added to the electrostatic interaction (static-exchange approximation). Elastic DCSs and spin-polarization functions can then be calculated by using the relativistic (Dirac) partial-wave expansion method. With the aid of available numerical algorithms (see, e.g., Ref. [5]), this kind of calculation is feasible for energies up to ~ 10 MeV. DCSs and spin-polarization functions calculated from the static-field

(or static-exchange) approximation agree well with available experimental data in this energy range; the differences are frequently of the same order of magnitude as the uncertainties in the measured data.

When the kinetic energy of the projectile decreases below ~ 5 keV, the accuracy of the static-field and static-exchange approximations deteriorates progressively. We recall that these approximations can be regarded as equivalent to the first-order term of a perturbative expansion of the transition matrix. The effect of second-order terms increases when the energy of the projectile decreases and can be accounted for approximately by using optical models [6–12], in which the interaction is described by means of a local complex potential. An optical-model potential consists of the static field (electrostatic interaction, with a local exchange correction in the case of electrons), the correlation-polarization potential (which accounts for the polarization of the target charge distribution under the action of the electric field of the projectile), and an absorptive imaginary potential (which describes the loss of flux due to the coupling with inelastic channels). For projectiles with relatively low energy, up to a few hundred eV, very accurate elastic DCSs can be obtained from coupled-channel optical calculations [13,14], in which a finite set of scattering channels is treated with the coupled-channel formalism and the rest of the channels are taken into account by means of an approximate nonlocal complex polarization potential (see, e.g., Refs. [13,14]). At these energies, convergent close-coupling calculations have also been performed for selected elements (see Ref. [15], and references therein).

Optical models provide a convenient methodology for elastic-scattering calculations at intermediate energies (from ~ 100 eV to ~ 5 keV), for which second-order effects are appreciable and more rigorous coupled-channel calculations are difficult due to the large number of open inelastic channels. Byron and Joachain [9] describe a systematic procedure

*Electronic address: cesc@ecm.ub.es

to construct the imaginary potential from an eikonal analysis of the second term of the Born series, which is evaluated approximately by closure. The calculation of the absorption potential by the eikonal-Born method requires knowledge of atomic wave functions and is fairly laborious. A number of groups have proposed simpler methods that require knowing only the atomic electron density, usually combined with some empirical information (e.g., total cross sections). For example, Furness and McCarthy [6] proposed an absorption potential that is proportional to the electron density and inversely proportional to the square of the “local” kinetic energy of the projectile. Staszewska *et al.* [11,12] have derived an absorption potential for electrons by considering the atomic electron cloud as an inhomogeneous electron gas, and assuming that inelastic collisions of the projectile are binary collisions described by the Rutherford DCS with Pauli-principle restrictions. This “quasifree” model has had quite remarkable success in describing elastic electron scattering at relatively low energies and has been recently generalized to the case of positron scattering by Reid and Wadehra [16]. However, the underlying model for binary collisions (Rutherford scattering with Pauli blocking) neglects electronic screening and the proposed absorption potential contains an empirical parameter that has a relatively strong influence on the potential.

Various approximate forms of local exchange and correlation-polarization potentials have been derived by means of the local-density approximation (LDA), i.e., by considering that each volume element of the target electron cloud behaves as if it were part of an homogeneous electron gas of the same density [17–19]. It has been established that these local potentials provide a fairly accurate description of exchange and polarization effects in elastic scattering of electrons and positrons by neutral atoms. The appeal of these approximations is that they can be applied to more complex systems such as molecules and solids, where close-coupling methods are impracticable. It is therefore natural to question whether the LDA is also capable of describing absorption effects accurately. In the present paper, we consider a LDA to the absorption potential that is based on Lindhard’s [20] dielectric formalism, which accounts for the effect of Pauli blocking consistently. The Lindhard theory also accounts for Debye screening, an effect which is disregarded in the quasifree model. In the case of electron scattering, exchange effects are introduced in the absorption potential model by using the Born-Ochkur approximation [21–23]. To leave room for possible empirical corrections, the proposed absorption potential contains two parameters, the energy gap Δ , which should be of the order of the first excitation threshold of the target atom, and a global strength factor A_{abs} . The absorption potential is then completely determined by the local electron density of the target and the parameters Δ and A_{abs} . For the cases for which enough experimental information is available (mostly noble gases), the optimum values of these parameters (i.e., obtained by fitting experimental information) are found to be nearly independent of energy, thus confirming the physical consistency of the absorption model.

Our main objective here is to devise an optical-model potential with defined empirical parameters. The proposed

model is intended for systematic calculation of the electron and positron elastic-scattering databases required for Monte Carlo simulation of low-energy electron and positron transport in amorphous media. We concentrate on the energy range from ~ 100 eV to ~ 5 keV, which is of interest, e.g., in electron surface spectroscopy and microdosimetry. The details of the optical-model potential are described in Sec. II. The calculation of cross sections for binary collisions of the projectile with a homogeneous electron gas, which are needed to obtain the absorption potential, is described in the Appendix. In Sec. III, we briefly consider the required modifications of a conventional Dirac partial-wave method to compute phase shifts for a complex central field and we introduce the set of observables that are calculated by our computer code. In Sec. IV, we analyze the dependence of the calculated DCSs on the model parameters and justify the selection of default values for these parameters. Section V contains a fairly extensive comparison of calculation results with available experimental data for scattering by noble gases and mercury. Sec. VI contains some concluding remarks.

II. OPTICAL POTENTIAL

As mentioned above, elastic scattering of electrons and positrons with kinetic energy E larger than ~ 5 keV is accurately described by the static-field approximation. Within this approximation, the structure of the target atom, of atomic number Z , is fully characterized by giving the nuclear and electronic charge distributions. For projectiles with energies less than ~ 10 MeV, the nucleus can be represented as a point charge. The electronic density $\rho(r)$ of free atoms (averaged over degenerate states in the case of open shells) is spherically symmetrical; the electron densities used in the present calculations were generated by means of the multi-configuration Dirac-Fock code of Desclaux [24]. The potential energy of the projectile at a distance r from the nucleus of the target atom is given by

$$V_{\text{st}}(r) \equiv \frac{Z_0 Z e^2}{r} - Z_0 e^2 \left(\frac{1}{r} \int_0^r \rho(r') 4\pi r'^2 dr' + \int_r^\infty \rho(r') 4\pi r' dr' \right), \quad (1)$$

where e is the absolute value of the electron charge and $Z_0 e$ is the charge of the projectile.

When the projectile is an electron, we must account for the occurrence of rearrangement collisions, in which the projectile exchanges places with an atomic electron. A convenient method to handle electron exchange effects is to replace the nonlocal exchange interaction by an approximate local potential (see, e.g., Ref. [4], and references therein). In the present calculations, we use the exchange potential of Furness and McCarthy [6,7,25], which is derived directly from the formal expression of the nonlocal exchange interaction by using a WKB-like approximation for the wave functions:

$$V_{\text{ex}}^{(-)}(r) = \frac{1}{2}[E - V_{\text{st}}(r)] - \frac{1}{2}\{[E - V_{\text{st}}(r)]^2 + 4\pi a_0 e^4 \rho(r)\}^{1/2}, \quad (2)$$

where a_0 is the Bohr radius. Bransden *et al.* [4] conclude that for scattering by H and He this effective potential describes exchange effects accurately for projectiles with kinetic energies larger than about 1 hartree.

A. Correlation-polarization potential

Slow projectiles cause the polarization of the charge cloud of the target atom and, in turn, the induced dipole moment acts back on the projectile. When the projectile is far from the atom, the polarization potential energy can be approximated by means of the Buckingham potential,

$$V_{\text{pol}}(r) = -\frac{\alpha_p e^2}{2(r^2 + d^2)^2}, \quad (3)$$

where α_p is the dipole polarizability of the target atom [26] and d is a phenomenological cutoff parameter, which serves to prevent the polarization potential from diverging at $r = 0$. Following Mittleman and Watson [27], we write

$$d^4 = \frac{1}{2} \alpha_p a_0 Z^{-1/3} b_{\text{pol}}^2 \quad (4)$$

and consider b_{pol} as an adjustable energy-dependent parameter, which can be determined by fitting the measured DCSs at small angles (see below). It is found that the magnitude of polarization effects decreases when the energy of the projectile increases (i.e., b_{pol} increases with E), reflecting the fact that atomic electrons do not react instantaneously to external electric fields. From a comparison of results from calculations using the potential $V_{\text{st}}(r) + V_{\text{ex}}^{(-)}(r) + V_{\text{pol}}(r)$ with available experimental DCS data for elastic scattering of electrons by atoms with $E \geq 100$ eV, Seltzer [28] suggested the following empirical formula:

$$b_{\text{pol}}^2 = (E - 50 \text{ eV}) / (16 \text{ eV}). \quad (5)$$

In what follows we shall use this recipe, which yields DCSs at small angles that are consistent with measurements for noble gases and mercury, and assume that the long-range polarization potential (3) is the same for electrons and positrons.

In a more elaborate model proposed by O'Connell and Lane [17], the short-range polarization field is obtained by using the LDA and assuming that the projectile is slow. The physical picture behind this model is that when the projectile penetrates the atomic volume its charge is dynamically screened by the atomic electrons. Thus, when the projectile is an electron, atomic electrons are repelled to form a "Coulomb hole" surrounding the projectile position, an effect which is usually referred to as "correlation." According to the LDA, the correlation energy of the projectile at r is the same as if it were moving within a free-electron gas of density ρ equal to the local atomic electron density. Following Padial and Norcross [18], the correlation potential $V_{\text{co}}(r)$ is calculated as the functional derivative of the free-electron-

gas correlation energy with respect to ρ . It is customary to express this potential as a function of the density parameter

$$r_s \equiv \frac{1}{a_0} \left[\frac{3}{4\pi\rho(r)} \right]^{1/3}, \quad (6)$$

which is the radius of the sphere that contains (on an average) one electron of the gas, in units of the Bohr radius a_0 . For electrons, we shall use the parametrization of the correlation potential given by Perdew and Zunger [29],

$$V_{\text{co}}^{(-)}(r) = -\frac{e^2}{a_0} (0.0311 \ln r_s - 0.0584 + 0.00133 r_s \ln r_s - 0.0084 r_s) \quad (7a)$$

for $r_s < 1$, and

$$V_{\text{co}}^{(-)}(r) = -\frac{e^2}{a_0} \beta_0 \frac{1 + (7/6)\beta_1 r_s^{1/2} + (4/3)\beta_2 r_s}{(1 + \beta_1 r_s^{1/2} + \beta_2 r_s)^2} \quad (7b)$$

for $r_s \geq 1$, where $\beta_0 = 0.1423$, $\beta_1 = 1.0529$ and $\beta_2 = 0.3334$. For positrons, we use the parametrization of the correlation potential proposed by Jain [19]:

$$V_{\text{co}}^{(+)}(r) = \frac{e^2}{a_0} \{0.5835 + 0.91 r_s^{-1/2} + [0.00255 \ln(r_s) - 0.0575] \ln(r_s)\} \quad (8a)$$

for $r_s < 0.302$,

$$V_{\text{co}}^{(+)}(r) = \frac{e^2}{a_0} [0.461525 - 0.04549 r_s^{-2}] \quad (8b)$$

for $0.302 \leq r_s < 0.56$,

$$V_{\text{co}}^{(+)}(r) = \frac{e^2}{a_0} \left[-\frac{4.3637}{(r_s + 2.5)^3} + \frac{-6.5755 + 0.4776 r_s}{(r_s + 2.5)^2} + \frac{1.43275}{r_s + 2.5} - 0.3149 \right] \quad (8c)$$

for $0.56 \leq r_s < 8$, and

$$V_{\text{co}}^{(+)}(r) = \frac{e^2}{a_0} [-15375.8679 r_s^{-6} + 44.5047 r_s^{-3} - 0.262] \quad (8d)$$

for $r_s \geq 8$. It is worth stressing the fact that these parametrized potentials correspond to slow projectiles; the correlation potential increases (decreases in magnitude) when the velocity of the projectile increases, and tends to zero at high energies.

To obtain the global correlation-polarization potential $V_{\text{cp}}^{(\pm)}(r)$, we consider that (1) at large distances it must reduce to the long-range polarization potential $V_{\text{pol}}(r)$ and (2) at small radii, where the atomic electron density is large, the LDA correlation potential given by Eqs. (7) and (8) is a lower bound for $V_{\text{cp}}^{(\pm)}(r)$. Accordingly, we set

$$V_{\text{cp}}^{(\pm)}(r) \equiv \begin{cases} \max\{V_{\text{co}}^{(\pm)}(r), V_{\text{pol}}(r)\} & \text{if } r < r_{\text{cp}}, \\ V_{\text{pol}}(r) & \text{if } r \geq r_{\text{cp}}, \end{cases} \quad (9)$$

where r_{cp} is the outer radius at which $V_{\text{co}}^{(\pm)}(r)$ and $V_{\text{pol}}(r)$ cross. Notice that the correlation potential for electrons, Eqs. (7), tends to zero for large r and, therefore, definition (9) is unambiguous, i.e., the potentials $V_{\text{co}}^{(\pm)}(r)$ and $V_{\text{pol}}(r)$ cross at least once. For positrons, when r increases, the potential $V_{\text{co}}^{(+)}(r)$, Eqs. (8), tends to a constant value (-0.262 hartree, which is the binding energy of the positronium negative ion). At high energies, the empirical polarization potential (3) is larger than $V_{\text{co}}^{(+)}(r)$ for all r and $V_{\text{cp}}^{(+)}(r)$ is set equal to $V_{\text{pol}}(r)$. With Seltzer's recipe, Eq. (5), the correlation-polarization potential defined by Eq. (9) is free from fitting parameters.

B. Absorption potential

For projectiles with kinetic energy above the first excitation threshold, there is a loss of flux from the elastic channel to inelastic channels. To model this effect, the optical potential must contain a negative imaginary part $-iW_{\text{abs}}(r)$. It can be easily shown that the quantity $(2/\hbar)W_{\text{abs}}(r)$ represents the absorption probability per unit time of the projectile at r (see, e.g., Ref. [30]). We can write an alternative expression for this absorption probability per unit time by invoking the LDA, i.e., considering that the projectile interacts as if it were moving within a homogeneous electrons gas of density $\rho(r)$ with velocity

$$v_L = (2E_L/m)^{1/2} \quad (10)$$

corresponding to the local kinetic energy

$$E_L(r) = \begin{cases} E - V_{\text{st}}(r) - V_{\text{ex}}^{(-)}(r) & \text{for electrons,} \\ \max(E - V_{\text{st}}(r), 0) & \text{for positrons.} \end{cases} \quad (11)$$

Assuming that the interactions with the electron gas are binary collisions, the LDA predicts an interaction probability per unit time equal to $v_L \rho \sigma_{\text{bc}}(E_L, \rho, \Delta)$, where $\sigma_{\text{bc}}(E_L, \rho, \Delta)$ is the cross section (per electron in the gas) for collisions involving energy transfers greater than the energy gap Δ . Notice that $\rho \sigma_{\text{bc}}(E_L, \rho, \Delta)$ is the inverse mean free path (i.e., the interaction probability per unit path length) of the projectile in the electron gas. Consequently, we set

$$W_{\text{abs}} = A_{\text{abs}} \hbar \frac{1}{2} (2E_L/m)^{1/2} \rho \sigma_{\text{bc}}(E_L, \rho, \Delta), \quad (12)$$

where A_{abs} is an empirical parameter, which should be of the order of unity. The factor $\frac{1}{2}$ in this equation comes from the interpretation of $(2/\hbar)W_{\text{abs}}(r)$ as the probability of absorption per unit time. This factor has nothing to do with exchange corrections, as incorrectly stated by various authors, and must be used for both electrons and positrons.

The energy gap Δ in Eq. (12) is introduced to account for the fact that excitations of the target atom are possible only when the energy W lost by the projectile is larger than the first inelastic threshold. For electron scattering, inelastic channels are open when the energy of the projectile is larger

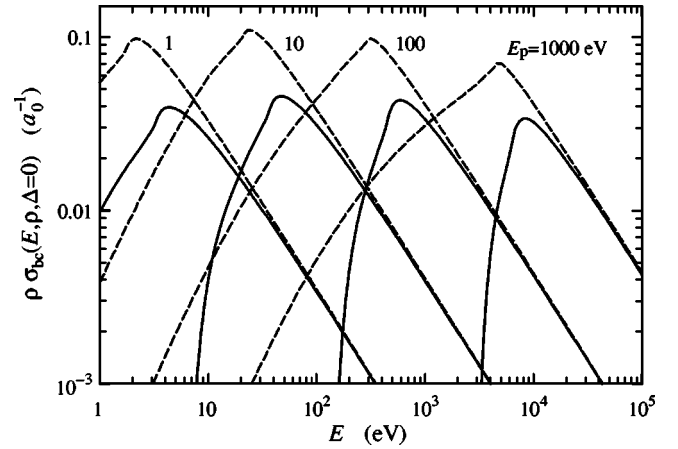


FIG. 1. Inverse mean free paths for binary collisions of electrons (solid curves) and positrons (dashed curves) moving with kinetic energy E in free-electron gases of various densities, corresponding to the indicated values of the plasma energy E_p .

than the first excitation energy ϵ_1 of the target atom and, accordingly, we should set $\Delta = \epsilon_1$. In the case of positron scattering, positronium formation is often the first inelastic channel to open. For atoms whose ionization potential I is larger than the positronium binding energy $|E_{1s}| \sim 6.8$ eV (such as the noble gases), the threshold energy for positronium formation is $\epsilon_{\text{ps}} = I - |E_{1s}|$. For atoms with $I < 6.8$ eV, positronium formation is possible at all energies, i.e., $\epsilon_{\text{ps}} = 0$. Hence, for positron scattering we should set $\Delta = \epsilon_{\text{ps}}$.

To describe the binary collisions of the projectile with the local free-electron gas we use the Born approximation with the generalized oscillator strength obtained from Lindhard's dielectric function, as described in the Appendix. This theory accounts for the effects of Pauli blocking and electronic screening consistently. However, in the case of electron scattering the Born-Lindhard formulation disregards the effect of electron exchange in inelastic interactions. To describe this effect, we employ the Born-Ochkur approximation [21–23], which yields the correct DCS for collisions with free electrons at rest. Figure 1 displays calculated inverse mean free paths $\rho \sigma_{\text{bc}}(E, \rho, \Delta)$ with $\Delta = 0$ for binary collisions with free-electron gases of various densities, corresponding to the indicated values of the plasma energy [see Eq. (6)] $E_p = (4\pi\rho e^2 \hbar^2/m)^{1/2}$, as functions of the kinetic energy E of the projectile. For kinetic energies larger than $\sim 100E_p$, the cross sections for electrons and positrons are approximately equal. For lower energies, the cross sections for electrons are smaller due to the effects of Pauli blocking and electron exchange. For positrons with kinetic energy below the plasmon excitation threshold ($\sim E_p$), the cross section decreases when the kinetic energy of the projectile decreases due to the screening of the projectile charge by the gas electrons.

It is worth stressing the fact that we are considering only binary (close) collisions of the projectile with the local electron gas and, therefore, neglecting the effect of plasmonlike interactions. The same is true for the quasifree model of Staszewska *et al.* [11,12]. Plasmonlike excitations involve relatively small momentum transfers and correspond to dis-

tant (dipolelike) interactions. In the case of low-energy projectiles, the probability of distant interactions with a target atom can be even larger than that of close collisions. Due to their delocalized character, it is not clear that how distant interactions can be described in terms of a local potential determined by only the atomic electron density. To account for the global effect of distant interactions, we shall consider A_{abs} as an empirical parameter and allow it to take values larger than unity.

Summarizing, the optical-model potentials for electrons and positrons obtained from the present LDA formulation are given by

$$V^{(-)}(r) = V_{\text{st}}(r) + V_{\text{ex}}^{(-)}(r) + V_{\text{cp}}^{(-)}(r) - iW_{\text{abs}}(r) \quad (13)$$

and

$$V^{(+)}(r) = V_{\text{st}}(r) + V_{\text{cp}}^{(+)}(r) - iW_{\text{abs}}(r), \quad (14)$$

respectively. The static, exchange, and correlation potentials are free of adjustable parameters. The long-range polarization potential contains the cutoff parameter b_{pol} , which has been empirically determined. The absorption potential (12) depends on the energy gap Δ and the strength parameter A_{abs} . We shall show below that with Δ equal to the first inelastic threshold and $A_{\text{abs}} \sim 2$, the present optical-model potential yields DCSs for elastic scattering of electrons by noble gases and mercury that are in good agreement with available experimental data for projectiles with kinetic energy larger than ~ 100 eV (see Sec. V). Calculation results also reveal that exchange, correlation-polarization, and absorption effects are appreciable only for projectile electrons and positrons with kinetic energies less than about 5 keV. Moreover, these corrections are important only for relatively large radial distances, because at small radii the interaction is dominated by the intense Coulomb field of the nucleus. Therefore, it is legitimate to use nonrelativistic quantum theory, as we have done here, to derive local corrections to the static potential $V_{\text{st}}(r)$.

III. THE DIRAC PARTIAL-WAVE ANALYSIS

The spherical symmetry of the potentials (13) and (14) allows the elastic DCSs to be calculated by using conventional partial-wave expansion methods. As indicated above, positrons are repelled by the nucleus and can only “see” the outer part of the atom. As a consequence, DCSs for elastic scattering of slow positrons could be calculated by solving the nonrelativistic Schrödinger equation. This is not the case for electrons, which are attracted by the Coulomb field of the nucleus and can reach large velocities at small radial distances, a fact that requires the use of the Dirac equation to compute elastic-scattering DCSs and spin-polarization functions. However, as the numerical effort required to solve the Schrödinger equation is not significantly less than the effort needed to solve the Dirac equation, we shall use the latter for both electrons and positrons.

The scattering of relativistic electrons or positrons by a central field $V(r)$ (real or complex) is completely described

by the direct and spin-flip scattering amplitudes, given by [3,31]

$$f(\theta) = \frac{1}{2ik} \sum_{\ell} \{(\ell+1)[\exp(2i\delta_{\kappa=-\ell-1}) - 1] + \ell[\exp(2i\delta_{\kappa=\ell}) - 1]\} P_{\ell}(\cos\theta) \quad (15)$$

and

$$g(\theta) = \frac{1}{2ik} \sum_{\ell} [\exp(2i\delta_{\kappa=\ell}) - \exp(2i\delta_{\kappa=-\ell-1})] P_{\ell}^1(\cos\theta), \quad (16)$$

respectively. k is the relativistic wave number of the projectile, which is related to the kinetic energy E by

$$(c\hbar k)^2 = E(E + 2m_e c^2), \quad (17)$$

where c is the velocity of light in vacuum. $P_{\ell}(\cos\theta)$ and $P_{\ell}^1(\cos\theta)$ are Legendre polynomials and associated Legendre functions, respectively.

A. Numerical calculation of the phase shifts

The phase shifts δ_{κ} represent the large- r behavior of the Dirac spherical waves (see, e.g., Ref. [32])

$$\psi_{E\kappa m}(\mathbf{r}) = \frac{1}{r} \begin{pmatrix} P_{E\kappa}(r)\Omega_{\kappa,m}(\hat{\mathbf{r}}) \\ iQ_{E\kappa}(r)\Omega_{-\kappa,m}(\hat{\mathbf{r}}) \end{pmatrix}, \quad (18)$$

where $\Omega_{\kappa,m}(\hat{\mathbf{r}})$ are the spherical spinors and the radial functions $P_{E\kappa}(r)$ and $Q_{E\kappa}(r)$ satisfy the coupled system of differential equations [32]

$$\begin{aligned} \frac{dP_{E\kappa}}{dr} &= -\frac{\kappa}{r}P_{E\kappa} + \frac{E - V + 2m_e c^2}{c\hbar}Q_{E\kappa}, \\ \frac{dQ_{E\kappa}}{dr} &= -\frac{E - V}{c\hbar}P_{E\kappa} + \frac{\kappa}{r}Q_{E\kappa}. \end{aligned} \quad (19)$$

The relativistic quantum number κ is defined as $\kappa = (\ell - j)(2j + 1)$, where j and ℓ are the total and orbital angular-momentum quantum numbers, which are both determined by the value of κ ; $j = |\kappa| - 1/2$, $\ell = j + \kappa/(2|\kappa|)$.

In the present calculations, the phase shifts are obtained from the numerical solution of the radial equations (19) using the subroutine package RADIAL [33], which has been extended to cover the case of complex spherical potentials. The function $rV^{(\pm)}(r)$ is replaced by the natural cubic spline that interpolates the values of this function for a given grid of radii, dense enough to ensure that interpolation errors have a negligible effect on the computed radial functions. The integration of the radial equations is started at $r=0$, where $P_{E\kappa}(0) = Q_{E\kappa}(0) = 0$, and extended outwards up to a distance r_{∞} beyond the effective range of the interaction potential. In the interval between consecutive grid points, the radial functions are determined from their exact power-series expansions, which are summed up to the desired accuracy.

With this method truncation errors are completely avoided and, therefore, the radial functions are only affected by unavoidable round-off errors.

When $V(r)=0$, the radial functions reduce to familiar forms (see, e.g., Ref. [32])

$$\begin{aligned}
 P_{E\kappa}^{0,r}(r) &= kr j_{\kappa}(kr), \\
 Q_{E\kappa}^{0,r}(r) &= \left(\frac{E}{E+2m_e c^2} \right)^{1/2} kr j_{\kappa-1}(kr) \quad \text{if } \kappa > 0, \\
 P_{E\kappa}^{0,r}(r) &= kr j_{-\kappa-1}(kr), \\
 Q_{E\kappa}^{0,r}(r) &= - \left(\frac{E}{E+2m_e c^2} \right)^{1/2} kr j_{-\kappa}(kr) \quad \text{if } \kappa < 0,
 \end{aligned} \tag{20a}$$

where $j_{\ell}(x)$ are spherical Bessel functions. For the null potential and $r > 0$, the radial equations admit a second independent solution, which is irregular at $r=0$,

$$\begin{aligned}
 P_{E\kappa}^{0,i}(r) &= -kr n_{\kappa}(kr), \\
 Q_{E\kappa}^{0,i}(r) &= - \left(\frac{E}{E+2m_e c^2} \right)^{1/2} kr n_{\kappa-1}(kr) \quad \text{if } \kappa > 0,
 \end{aligned}$$

$$P_{E\kappa}^{0,i}(r) = -kr n_{-\kappa-1}(kr),$$

$$Q_{E\kappa}^{0,i}(r) = \left(\frac{E}{E+2m_e c^2} \right)^{1/2} kr n_{-\kappa}(kr) \quad \text{if } \kappa < 0, \tag{20b}$$

where $n_{\ell}(x)$ are spherical Neumann functions. To calculate the phase shift δ_{κ} , the numerical solution for $r \geq r_{\infty}$ is expressed as a linear combination of the regular and irregular solutions for the free particle,

$$P_{E\kappa}(r) = \cos(\delta_{\kappa}) P_{E\kappa}^{0,r}(r) + \sin(\delta_{\kappa}) P_{E\kappa}^{0,i}(r) \tag{21}$$

or, equivalently,

$$\begin{aligned}
 P_{E\kappa}(r) &= \exp(i\delta_{\kappa}) \frac{1}{2} [P_{E\kappa}^{0,r}(r) - iP_{E\kappa}^{0,i}(r)] \\
 &+ \exp(-i\delta_{\kappa}) \frac{1}{2} [P_{E\kappa}^{0,r}(r) + iP_{E\kappa}^{0,i}(r)].
 \end{aligned} \tag{22}$$

The phase shift δ_{κ} is determined by matching this outer analytical form to the inner numerical solution at r_{∞} , requiring continuity of the radial function $P_{E\kappa}(r)$ and its derivative. This gives

$$\exp(2i\delta_{\kappa}) = \frac{D_{\text{out}}[P_{E\kappa}^{0,r}(r_{\infty}) + iP_{E\kappa}^{0,i}(r_{\infty})] - [(P_{E\kappa}^{0,r})'(r_{\infty}) + i(P_{E\kappa}^{0,i})'(r_{\infty})]}{[(P_{E\kappa}^{0,r})'(r_{\infty}) - i(P_{E\kappa}^{0,i})'(r_{\infty})] - D_{\text{out}}[P_{E\kappa}^{0,r}(r_{\infty}) - iP_{E\kappa}^{0,i}(r_{\infty})]}, \tag{23}$$

where the primes indicate derivatives with respect to r and $D_{\text{out}} \equiv P'_{E\kappa}(r_{\infty})/P_{E\kappa}(r_{\infty})$ is the logarithmic derivative of the outgoing numerical radial function at the matching point. Formula (23) gives the phase coefficients $\exp(2i\delta_{\kappa})$ for arbitrary finite-range complex potentials. The phase shifts of a real potential are all real. When the potential is complex, the phase shifts are also complex; their imaginary part decreases when $|\kappa|$ increases because, for sufficiently large angular momenta, the centrifugal barrier prevents the projectile from perceiving the short-range imaginary potential.

The calculations presented here have been performed with a FORTRAN 77 code, in which all real variables are represented in double precision. When ℓ is sufficiently large, the absolute value of the phase shift decreases monotonously with ℓ . Our computer code calculates phase shifts for increasing orders ℓ up to a certain value ℓ_{max} for which δ_{κ} becomes smaller than $\sim 10^{-8}$. At this point, the partial-wave expansions (15) and (16) have converged to the required accuracy (usually more than six decimal places) for all angles. It is convenient to mention here that, due to the long-range polarization potential, the absolute value of the phase shift decreases very slowly with ℓ . A simple trick to speed up the calculation consists of neglecting the polarization potential for large r , where it becomes negligible in comparison with

E . In the present calculations when $r > 50a_0$ and $|V_{\text{cp}}^{(\pm)}(r)| < 10^{-6}E$, we set $V^{(\pm)}(r) = 0$. This truncation of the potential allows a considerable reduction of the computation time and only affects the DCS at very small angles ($\approx 2^\circ$), where it is slightly underestimated.

B. Observable quantities

Our computer code delivers the scattering amplitudes, the elastic DCS, the total (integrated) elastic cross section, and Sherman's spin-polarization function. For the usual case of electron and positron beams that are not spin polarized, the DCS for elastic scattering is

$$\frac{d\sigma}{d\Omega} = |f(\theta)|^2 + |g(\theta)|^2. \tag{24}$$

The total elastic cross section is

$$\sigma_{\text{el}} = \int \frac{d\sigma}{d\Omega} d\Omega = 2\pi \int_0^\pi [|f(\theta)|^2 + |g(\theta)|^2] \sin\theta d\theta. \tag{25}$$

The code also delivers the momentum-transfer cross section

$$\sigma_{\text{mt}} = \int \frac{d\sigma}{d\Omega} (1 - \cos \theta) d\Omega, \quad (26)$$

which plays an important role in the simulation of electron-positron transport processes. Scattering amplitudes and DCSs are tabulated for a grid of angles, which is dense enough to allow the integrals to be evaluated by means of log-log interpolation.

Elastic scattering causes the spin polarization of initially unpolarized beams [3]. The degree of polarization of projectiles scattered in the direction θ is given by the Sherman function

$$S(\theta) \equiv i \frac{f(\theta)g^*(\theta) - f^*(\theta)g(\theta)}{|f(\theta)|^2 + |g(\theta)|^2}. \quad (27)$$

For certain target atoms and projectile kinetic energies, the absolute value of $S(\theta)$ is close to unity at specific scattering angles. Under these circumstances elastic scattering produces highly polarized electron beams, although their intensity is relatively small. The Sherman function is experimentally determined by means of double-scattering experiments [34,35].

IV. DEPENDENCE ON THE PARAMETERS

We have performed extensive comparisons of electron elastic DCSs calculated with the static-exchange (SE) potential $V_{\text{st}}(r) + V_{\text{ex}}^{(-)}(r)$ and with the SE plus correlation-polarization (SECP) potential $V_{\text{st}}(r) + V_{\text{ex}}^{(-)}(r) + V_{\text{cp}}^{(-)}(r)$, using experimental values of the dipole atomic polarizability α_p [26]. For projectiles with kinetic energies larger than ~ 500 eV, the effect of atomic polarization on the DCS is limited to small angles ($\theta < 15^\circ$) and decreases in magnitude when the value of the polarization cutoff parameter b_{pol} increases. For energies below 500 eV, the effect of the polarization potential extends to intermediate and larger angles and alters both the absolute value and the position of the minima of the DCS. The dependence of the DCS on b_{pol} is illustrated in Fig. 2 for the case of 500-eV-electron scattering by argon atoms. The displayed DCSs were obtained from the SE potential and from the SECP potential with different values of b_{pol} . For angles larger than about 20° , the effect of the correlation-polarization correction is negligible for E larger than ~ 500 eV. When reliable measurements of the DCS at small angles are available, the cutoff parameter can be determined by fitting the data, even if these are relative. The empirical formula (5) was inferred from a comparison of similar calculations with a large amount of experimental data published by numerous authors on noble gases and mercury.

The effects of the absorption potential parameters A_{abs} and Δ on the DCSs are entangled. For kinetic energies E larger than ~ 500 eV and neutral atoms, Δ has a small influence on the DCS and, therefore, its precise value is not important. The effect of this parameter becomes more visible when the kinetic energy of the projectile decreases. Figure 3 displays DCSs for 100 eV electron scattering by argon atoms calculated with $\Delta = 0$ and with Δ equal to the first excitation energy (11.6 eV), both with $A_{\text{abs}} = 2$. Even at this relatively

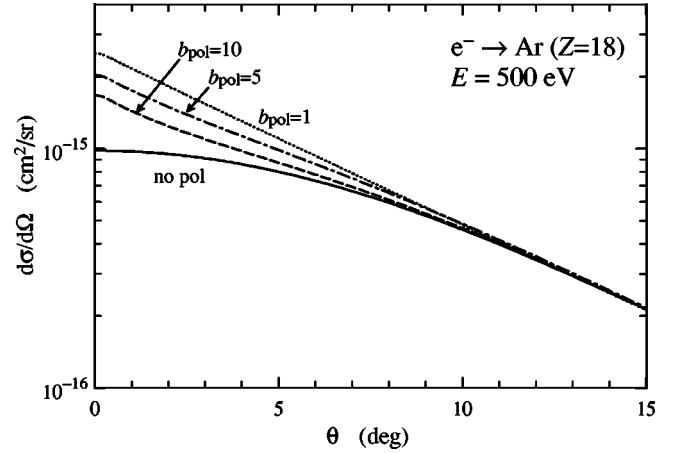


FIG. 2. Effect of the polarization cutoff parameter b_{pol} on the elastic DCS. The solid curve represents the DCS calculated with the SE potential. The other curves are DCSs obtained from the SECP potential with the indicated values of b_{pol} . For $\theta > 20^\circ$, they all practically coincide.

low energy, Δ has a small effect on the DCS. As indicated above, we shall set Δ equal to the threshold excitation energy for electrons and equal to the positronium formation threshold for positrons. This recipe may also be used to describe elastic scattering by positive ions. However, when the kinetic energy of the projectile is of the order of or less than the first excitation threshold, the energy gap is expected to have a more significant effect on the DCS. Nevertheless, in the extreme cases where $E < \Delta$ the optical-model potential reduces to the static-exchange plus correlation-polarization potential, which is the effective interaction expected when all inelastic channels are closed.

The strength A_{abs} of the absorption potential has a direct impact on the calculated DCS, the absorption correction being nearly proportional to A_{abs} . This correction alters the DCS predominantly at intermediate and large scattering

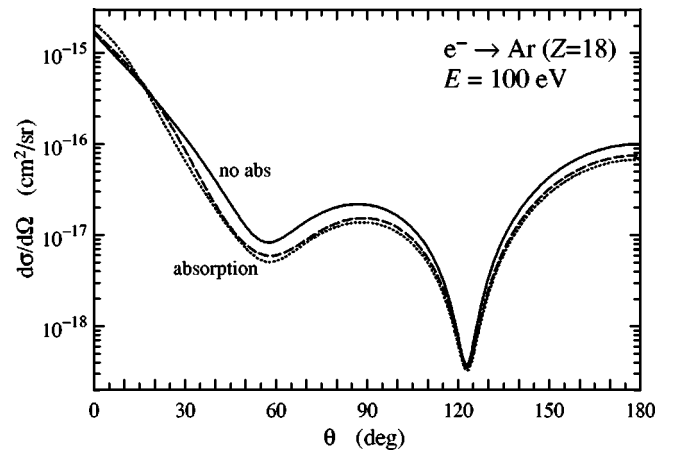


FIG. 3. Effect of the energy gap Δ on the calculated DCS. The solid curve represents the DCS obtained from the SECP potential with the empirical value of b_{pol} (i.e., with $A_{\text{abs}} = 0$). The dashed and dotted curves are the results from the optical-model potential with $\Delta = 11.6$ eV and with $\Delta = 0$, respectively, both with $A_{\text{abs}} = 2$.

angles and, therefore, the interference between correlation-polarization and absorption corrections is weak. This means that, with the adopted values of b_{pol} and Δ , A_{abs} can be determined by simply fitting the experimental DCSs at intermediate and large angles. From the experimental DCS data available for noble gases and mercury (see the following section), we have found that the value $A_{\text{abs}}=2$ provides a satisfactory description of elastic scattering of projectiles with kinetic energies larger than about 100 eV.

We would like to mention that at nonrelativistic energies, the grand total (elastic and absorption) cross section can be obtained from the optical theorem

$$\sigma_{\text{T}} \equiv \sigma_{\text{el}} + \sigma_{\text{abs}} = \frac{4\pi}{k} \text{Im}f(0). \quad (28)$$

As grand total cross sections are easier to measure than elastic differential and total cross sections, it may seem plausible to determine the parameter A_{abs} of the absorption potential (12) by requiring that the value of σ_{T} calculated from Eq. (28) agrees with available experimental data. This would yield a consistent description of both elastic and inelastic collisions whenever the adopted local absorption potential is a faithful representation of the true potential. As our LDA potential is only an approximation, this method is not expected to be of any practical use here and we have preferred to determine A_{abs} from experimental large-angle elastic DCS data.

V. COMPARISON WITH EXPERIMENTS

In Fig. 4 we compare calculated DCSs for elastic scattering of electrons ($100 \text{ eV} \leq E < 1 \text{ keV}$) by noble gases and mercury with available absolute experimental data. In these figures, the dashed curves represent results from the SE approximation and solid curves are results from the present optical-model potential with the parameter values recommended above, i.e., α_{p} from Ref. [26], b_{pol} given by Eq. (5), $A_{\text{abs}}=2$, and Δ equal to the first inelastic threshold. The adopted values of Δ for helium, neon, argon, krypton, xenon, and mercury are 19.8, 16.6, 11.6, 9.9, 8.3, and 4.7 eV, respectively [36]. It is seen that the SE approximation underestimates the DCS at small angles and overestimates it at large angles. Inclusion of the correlation-polarization potential increases the DCS at small angles to agree very closely with the experimental values. The absorption potential effectively reduces the DCS at larger angles, giving results that overall agree much better with measured data.

Figure 5 displays a similar comparison for noble gases and kinetic energies in the keV range. We see that our optical-model potential with the default parameter values reproduces the experimental data very accurately. Notice that the relative magnitude of correlation-polarization and absorption corrections decreases when the energy of the projectile increases. In practice, for $E > 5 - 10 \text{ keV}$ these corrections can be ignored. A good agreement is also found between calculated and measured total elastic cross section, Fig. 6, even for energies below 100 eV, which are outside the range where the model parameters have been fitted.

In principle, our method is also applicable to positron scattering. As the long-range polarization potentials are the same for electrons and positrons, calculations for positrons would only require determination of the absorption potential parameters. As in the case of electrons, the DCS depends very weakly on the energy gap Δ . To determine the parameter A_{abs} we would need experimental measurements of the DCS at large angles. As these are still very scarce, we tentatively use the value $A_{\text{abs}}=2$ obtained for electrons and set Δ equal to the positronium formation threshold, 8.96 eV for argon. Figure 7 compares DCSs calculated from the optical-model potential with the results of absolute measurements by Dou *et al.* [58] for elastic scattering of 100 and 300 eV positrons by argon atoms. DCSs calculated from the static plus correlation-polarization potential, $V_{\text{st}}(r) + V_{\text{cp}}(r)$, have a complicated structure at small angles, which is partially washed out when absorption is included.

Calculated Sherman functions for spin polarization in elastic electron scattering by the heavier noble gases and mercury are compared with experimental data in Fig. 8. Our results agree moderately well with the experiments for energies E larger than $\sim 100 \text{ eV}$. In the case of xenon and 50 eV, the calculation differs significantly from the measured data, indicating that our optical-model potential may be too simple to describe the interaction at this low energy. In general, for moderately high energies, the Sherman function is relatively insensitive to the correlation-polarization and absorption potentials. This can be understood by recalling that spin polarization is mostly due to spin-orbit coupling (see, e.g., Ref. [35]), which is appreciable only at relatively small radial distances, where the potential reduces essentially to the Coulomb field of the nucleus. The case of scattering of $\sim 150\text{-eV}$ electrons by xenon is interesting; we see that the SE calculation predicts a polarization peak near $\theta = 108^\circ$, in accordance with the optical-model calculation and experiment, but with reversed sign. Keeping aside this feature, the results of the two calculations are practically equivalent.

VI. CONCLUSION

The proposed optical-model potential and the associated computer code provide a complete description of elastic scattering of electrons and positrons of intermediate energies ($E > 100 \text{ eV}$) by atoms. Apart from the parameters b_{pol} , Δ , and A_{abs} , the potential is completely determined by the local electron density. We have shown that, for projectiles with kinetic energy larger than $\sim 100 \text{ eV}$, DCSs, total cross sections, and spin-polarization functions calculated with the “default” values of the model parameters agree well with experiments. With this set of parameters, calculated DCSs are substantially more accurate than those obtained from the static-field approximation, which are in common use in electron-transport simulations by Monte Carlo methods. The calculation of a complete database of DCSs for elastic scattering of electrons and positrons with kinetic energies from 100 eV to 10 keV by neutral atoms ($Z=1-103$) is in progress and will be made available in due course.

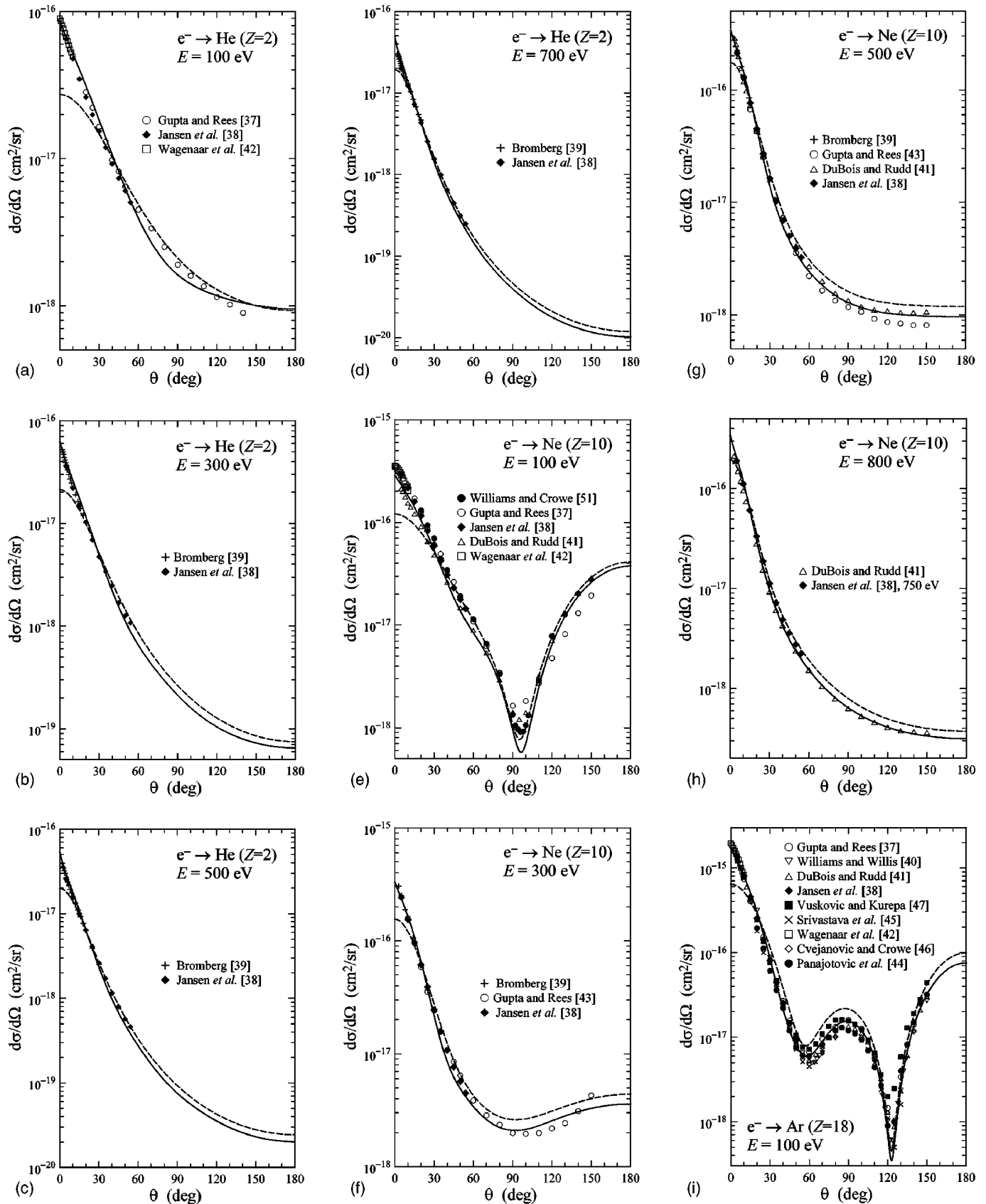


FIG. 4. Differential cross sections for elastic scattering of electrons by atoms of the elements helium, neon, argon, krypton, xenon, and mercury. Symbols represent experimental data from Refs. [37–55]. Solid curves are results from calculations with the present optical-model potential (13). The dashed curves represent results from similar calculations with the SE potential.

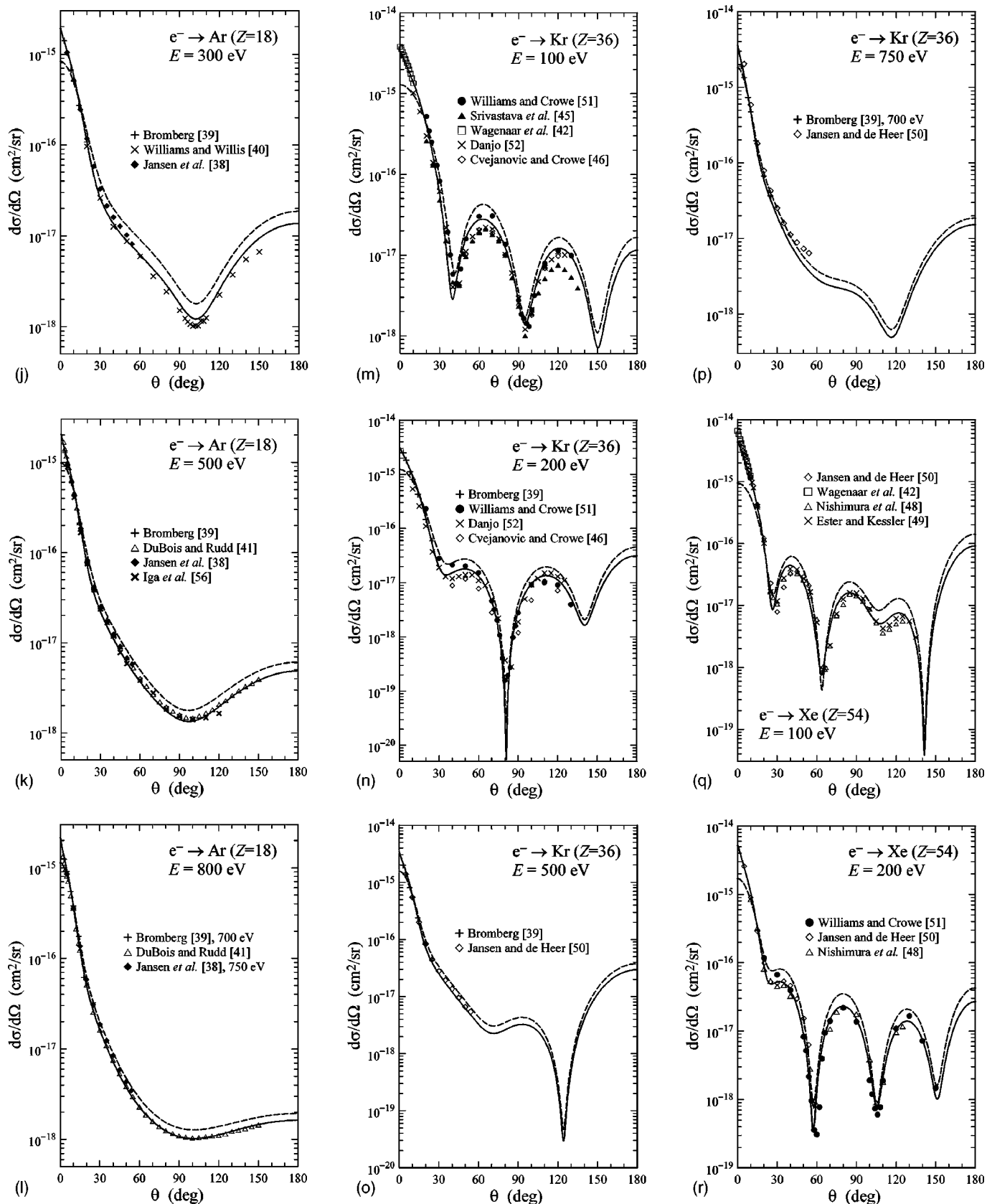


FIG. 4 (Continued).

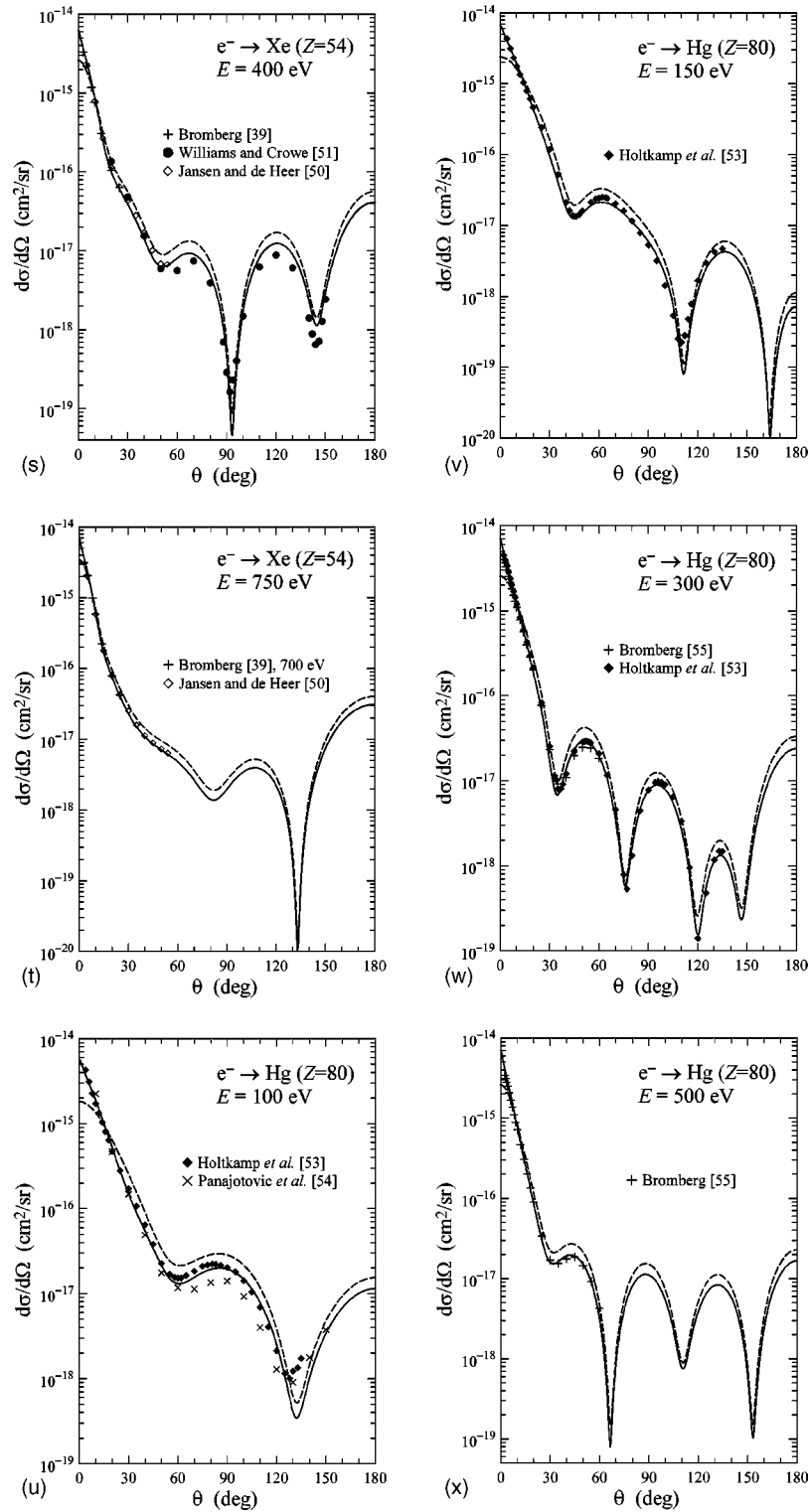


FIG. 4 (Continued).

ACKNOWLEDGMENTS

The author wishes to thank Cedric Powell, Mitio Inokuti, and David Liljequist for stimulating discussions, Stephen Seltzer for providing the empirical formula (5) for the polar-

ization cutoff parameter, José M. Fernández-Varea and Michael Dingfelder for comments on the manuscript and for verifying the numerical calculations, and Neus Salvat for helping with the plots. Financial support from the Fondo de Investigación Sanitaria (Spain), Project No. 01/0093, is gratefully acknowledged.

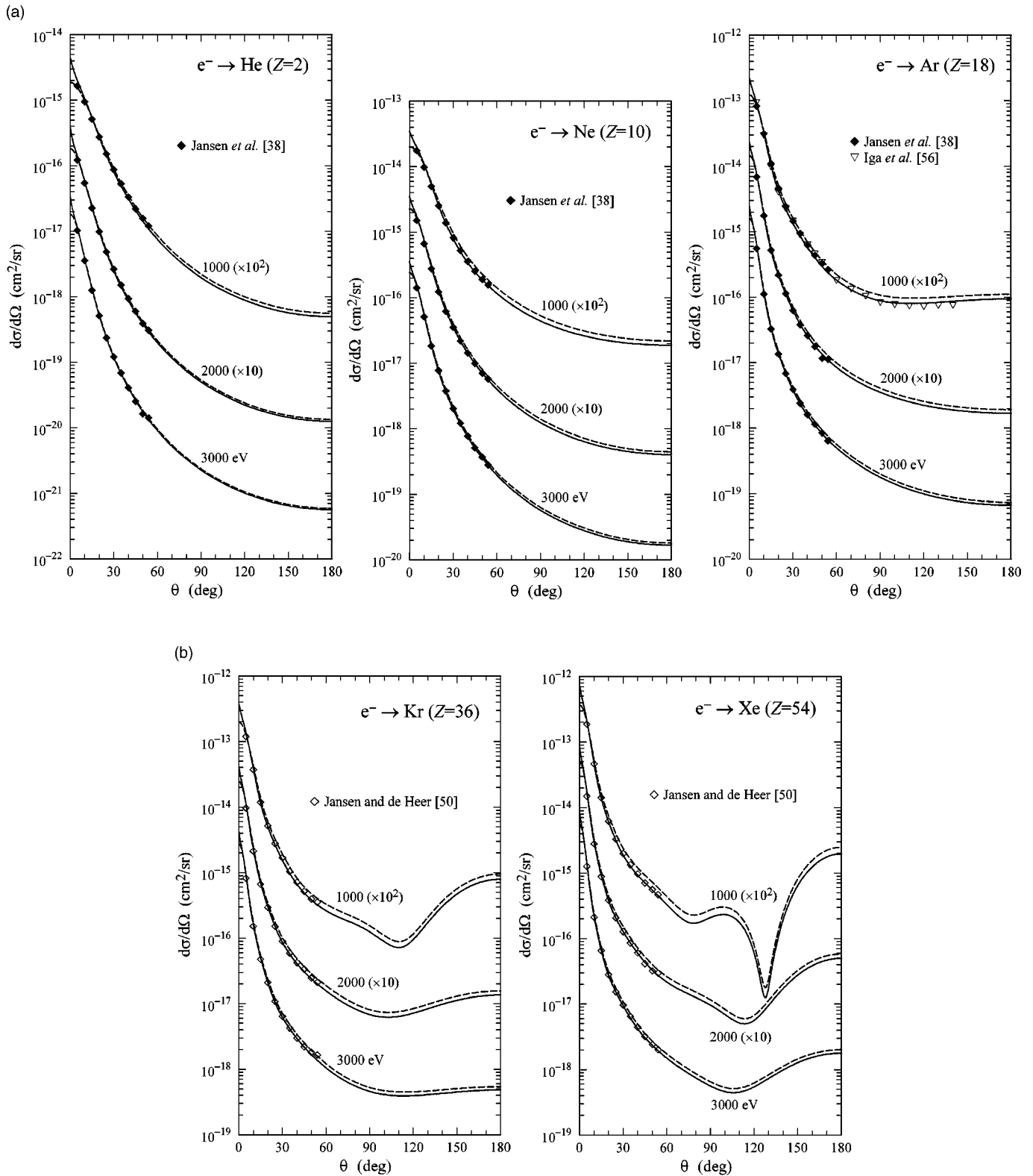


FIG. 5. DCSs for elastic scattering of electrons with $E=1, 2,$ and 3 keV by noble-gas atoms. Symbols represent experimental data from Refs. [38,50,56]. Solid curves are results from calculations with the present optical-model potential (13). The dashed curves represent results from similar calculations with the SE potential. For clarity, some of the DCSs have been multiplied by the indicated powers of ten.

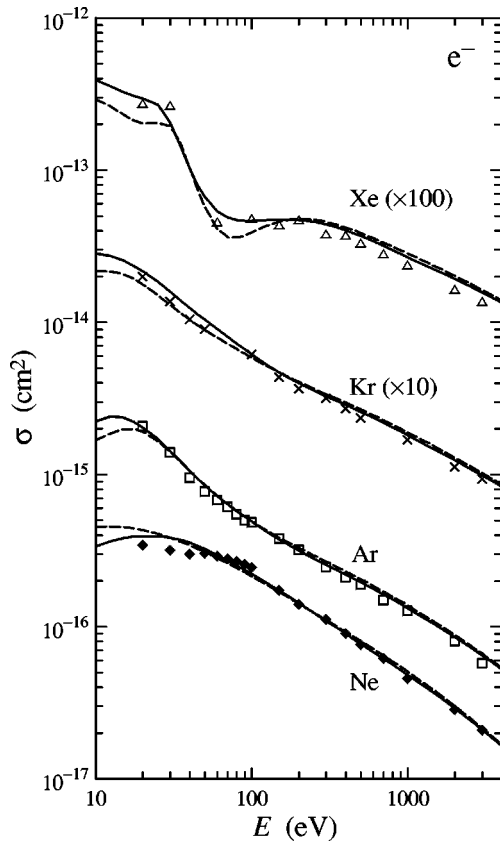


FIG. 6. Total (integrated) cross sections for elastic scattering of electrons by neon, argon, krypton, and xenon atoms, as functions of the kinetic energy of the projectile. Solid curves are results from the present optical-model potential and dashed curves are the results of calculations with the SE potential. Symbols represent semiempirical values obtained by de Heer *et al.* [57] from a compilation of experimental data of different authors.

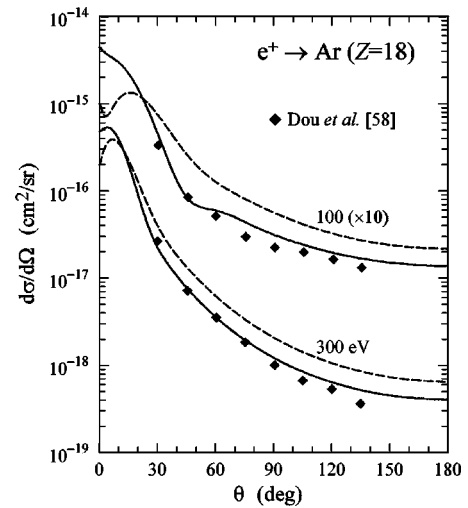


FIG. 7. DCSs for elastic scattering of 100 and 300 eV positrons by argon atoms. Symbols are experimental data from Ref. [58]. Solid curves are results from calculations with the present optical-model potential (14). The dashed curves represent results from similar calculations with the static plus correlation-polarization potential.

APPENDIX: CROSS SECTIONS FOR BINARY COLLISIONS WITH A FREE-ELECTRON GAS

The only nontrivial ingredient of the proposed optical-model potential is the one-electron cross section $\sigma_{bc}(E, \rho, \Delta)$, Eq. (12), for binary collisions of electrons and positrons of kinetic energy E with a degenerate free-electron gas (FEG) of density ρ (electrons per unit volume) involving energy losses larger than the energy gap Δ . The interactions with the FEG will be described by combining the dielectric theory of Lindhard [20] with the (nonrelativistic) first Born approximation (see, e.g., Ref. [64]). The latter leads to the

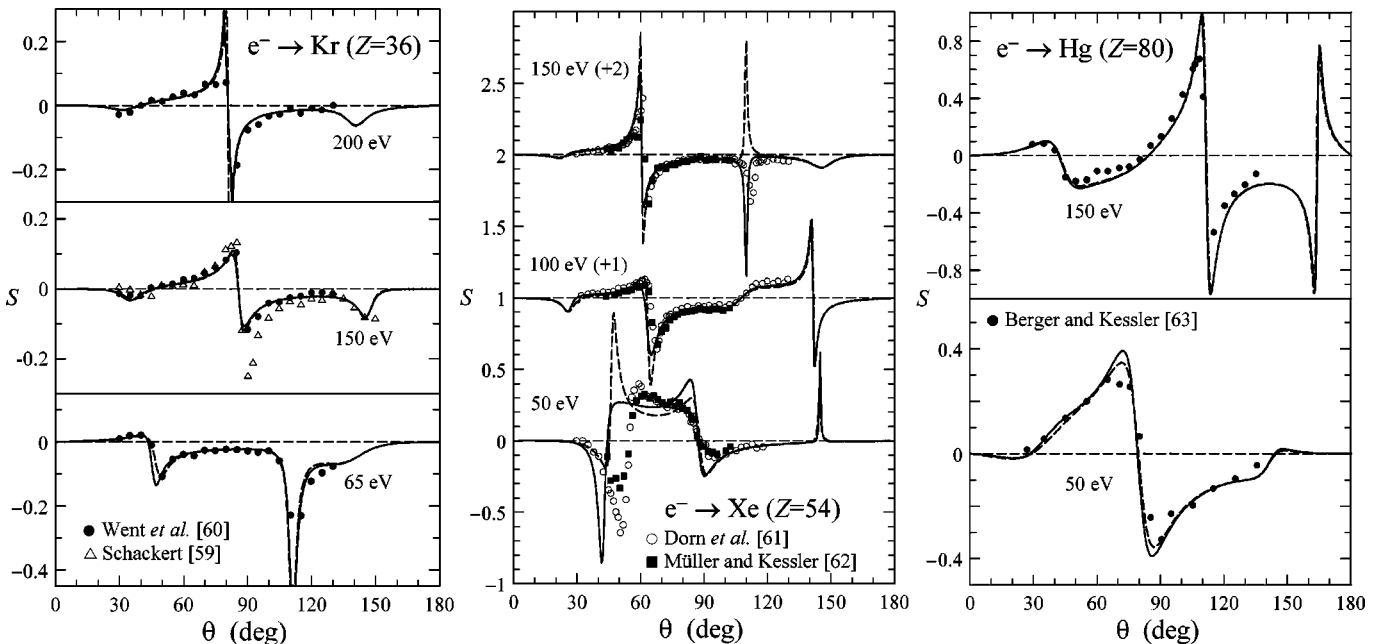


FIG. 8. Sherman function for elastic scattering of electrons with the indicated kinetic energies by krypton, xenon, and mercury atoms. Symbols are experimental data from Refs. [59–63]. Solid curves are results from calculations with the present optical-model potential (13); dashed curves represent results from calculations using the SE potential.

following expression for the DCS per electron in the gas:

$$\frac{d^2\sigma_{\text{feg}}}{dWdQ} = \frac{\pi e^4}{E} \frac{1}{WQ} \frac{df_L(Q,W)}{dW}, \quad (\text{A1})$$

where W is the energy transfer and Q , the so-called ‘‘recoil energy,’’ is defined by [64]

$$Q \equiv \frac{(\hbar q)^2}{2m_e} = E - W - 2\sqrt{E(E-W)}\cos\theta, \quad (\text{A2})$$

where $\hbar q$ is the magnitude of the momentum transfer and θ is the polar scattering angle. Notice that, for a given energy loss W , the kinematically allowed recoil energies lie in the interval between $Q_- = Q(W, \theta=0)$ and $Q_+ = Q(W, \theta=\pi)$,

$$Q_{\pm} = (\sqrt{E} \pm \sqrt{E-W})^2. \quad (\text{A3})$$

Conversely, for a given recoil energy, the interval of allowed energy losses extends from $W=0$ to

$$W = 2\sqrt{EQ} - Q. \quad (\text{A4})$$

The quantity $df_L(Q,W)/dW$ is the generalized oscillator strength (GOS) per electron of the FEG. Lindhard [20] used the random-phase approximation to derive a closed analytical expression for the dielectric function of the FEG, $\epsilon_L(q, \omega)$, which is a function of the wave number q and the angular frequency ω or, equivalently, of the recoil energy Q and the energy transfer $W = \hbar\omega$. Knowledge of the dielectric function allows the calculation of the energy loss per unit path length (stopping power) of charged particles in the FEG; the result is consistent with that of the Born approximation if we set

$$\frac{df_L(Q,W)}{dW} = \frac{2W}{\pi E_p^2} \frac{1}{Q} \text{Im}\left(\frac{-1}{\epsilon_L(Q,W)}\right), \quad (\text{A5})$$

where

$$E_p \equiv \sqrt{4\pi\rho e^2\hbar^2/m_e} = \sqrt{3}r_s^{-3} \frac{m_e e^4}{\hbar^2} \quad (\text{A6})$$

is the plasma energy of the FEG. It is convenient to introduce the Fermi energy,

$$E_F = \frac{\hbar^2}{2m_e} (3\pi^2\rho)^{2/3} = \frac{1}{2} \left(\frac{9\pi}{4}\right)^{2/3} r_s^{-2} \frac{m_e e^4}{\hbar^2}, \quad (\text{A7})$$

and the reduced variables [65]

$$x \equiv W/E_F \quad \text{and} \quad z \equiv \frac{1}{2}(Q/E_F)^{1/2}. \quad (\text{A8})$$

Expressed in terms of these variables the one-electron DCS of the FEG reads

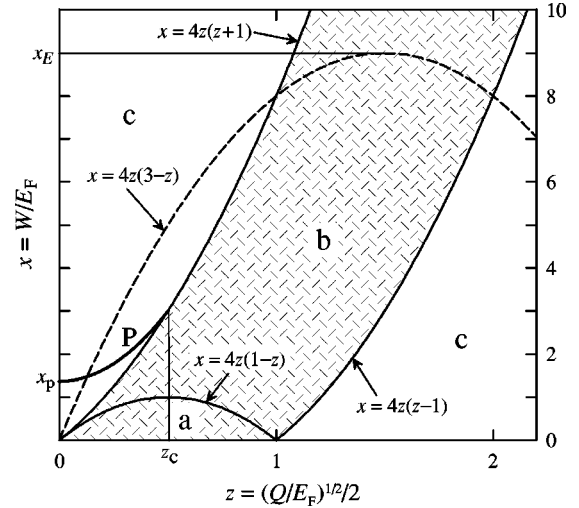


FIG. 9. Schematic representation of the GOS of a FEG. The shaded strip is the Lindhard continuum, which corresponds to electron-hole excitations. The resonance line P describes plasmon excitations; for $z=0$ the plasmon reduced energy is $x_p = E_p/E_F$. The dashed curve represents the energy-momentum conservation limit, Eq. (A26), for a projectile with kinetic energy $E=9E_F$. The kinematically allowed excitations lie below this curve.

$$\frac{d^2\sigma_{\text{feg}}}{dx dz} = \frac{2\pi e^4}{EE_F} \frac{1}{xz} \frac{df_L(z,x)}{dx} \quad (\text{A9})$$

with the GOS

$$\frac{df_L(z,x)}{dx} = \frac{6x}{16\pi\chi^2} \frac{z^2\chi^2 f_2(z,x)}{[z^2 + \chi^2 f_1(z,x)]^2 + \chi^4 f_2^2(z,x)}, \quad (\text{A10})$$

where

$$\chi^2 = \frac{3}{16} \left(\frac{E_p}{E_F}\right)^2 = \left(\frac{2}{3\pi^2}\right)^{2/3} r_s \quad (\text{A11})$$

and

$$f_1(z,x) = \frac{1}{2} + \frac{1}{8z} \left[1 - \left(z - \frac{x}{4z}\right)^2 \right] \ln \left| \frac{z-x/4z+1}{z-x/4z-1} \right| + \frac{1}{8z} \left[1 - \left(z + \frac{x}{4z}\right)^2 \right] \ln \left| \frac{z+x/4z+1}{z+x/4z-1} \right|. \quad (\text{A12})$$

The function $f_2(z,x)$ takes different expressions on different regions of the (z,x) plane (Fig. 9):

$$f_2(z,x) = \begin{cases} \frac{\pi x}{8z} & \text{if } |z+x/4z| \leq 1 \text{ (region } a), \\ \frac{\pi}{8z} [1 - (z-x/4z)^2] & \text{if } |z+x/4z| > 1 \text{ and } |z-x/4z| < 1 \text{ (region } b), \\ \tau g(z,x) & \text{if } |z-x/4z| \geq 1 \text{ (region } c), \end{cases} \quad (\text{A13})$$

where τ is a small positive constant, which is allowed to approach zero at the end of the calculations, and $g(z,x)$ is a function, whose exact form is irrelevant.

The GOS (A10) takes nonvanishing values in the region of the (z,x) plane limited by the curves $x=4z(z+1)$ and $x=4z(z-1)$ (see Fig. 9), the so-called Lindhard continuum, which represents electron-hole excitations. It can be easily verified that this is the domain of energy and momentum transfers that are kinematically allowed in binary collisions with the electrons of the gas (which move with an isotropic momentum distribution). The one-electron DCS for binary collisions $[(x,z) \in a \cup b]$ is given by

$$\frac{d^2\sigma_{bc}}{dx dz} = \frac{2\pi e^4}{EE_F} \frac{1}{xz} \frac{6}{16\pi\chi^2} \frac{z\chi^2 f_2(z,x)}{[z^2 + \chi^2 f_1(z,x)]^2 + \chi^4 f_2^2(z,x)}. \quad (\text{A14})$$

In region c , the GOS is equal to zero except in the neighborhood of the plasma resonance line P , where the denominator of expression (A10) vanishes. This line is defined by the implicit equation

$$P(z,x) \equiv z^2 + \chi^2 f_1(z,x) = 0, \quad (\text{A15})$$

and corresponds to excitation of longitudinal free oscillations of the gas, i.e., to plasmon excitation. In region c we have

$$\begin{aligned} \frac{df_L^{(c)}(z,x)}{dx} &= \frac{6}{16\pi\chi^2} xz^2 \lim_{\tau \rightarrow 0} \frac{\chi^2 \tau g(z,x)}{P^2(z,x) + \chi^4 \tau^2 g^2(z,x)} \\ &= \frac{6}{16\chi^2} xz^2 \delta[P(z,x)]. \end{aligned} \quad (\text{A16})$$

The plasmon cutoff momentum z_c is defined by the entrance of the plasma resonance line into the Lindhard continuum, i.e., as the root of the equation

$$P[z_c, 4z_c(z_c+1)] = 0. \quad (\text{A17})$$

The quantity

$$W_c = x_c E_F = 4z_c(z_c+1)E_F \quad (\text{A18})$$

is the maximum energy that can be absorbed by a plasmon without degenerating into electron-hole pairs. The DCS for binary collisions diverges at the point (z_c, x_c) . The DCS for plasmon excitation is given by

$$\frac{d^2\sigma_{pl}}{dx dz} = \frac{2\pi e^4}{EE_F} \frac{1}{xz} \frac{6}{16\chi^2} xz^2 \delta[P(z,x)], \quad z \leq z_c. \quad (\text{A19})$$

The kinematic allowed interactions correspond to points (z,x) in the region limited by the z axis and the energy- and momentum-conservation curve [cf. Eq. (A3)]

$$x = 4z(x_E^{1/2} - z), \quad x_E \equiv E/E_F. \quad (\text{A20})$$

For a positron, the maximum allowed energy loss in a single collision is equal to the kinetic energy of the projectile, i.e.,

$$x_{\max}^{(+)} = x_E. \quad (\text{A21})$$

When the projectile is an electron, the value of the maximum-energy loss is limited by Pauli's exclusion principle, which forbids transitions that would place the projectile into a filled state below the Fermi level, i.e., $x_{\max}^{(-)} = x_E - 1$. Moreover, electrons can undergo exchange interactions. The effect of these interactions, which is not included in the original Lindhard theory, can be accounted for by means of the Ochkur approximation [21–23], which is obtained by considering that the exchange scattering amplitude can be approximated by the leading term of an expansion of the Born-Oppenheimer amplitude in inverse powers of E . The Born-Ochkur DCS for interactions of an electron with the FEG is given by

$$\frac{d^2\sigma_{feg}}{dx dz} = \frac{2\pi e^4}{EE_F} \frac{1}{xz} \frac{df_L(z,x)}{dx} F_{ex}(z,x) \quad (\text{A22})$$

with

$$F_{ex}(z,x) = 1 - \frac{4z^2}{x_E - x} + \frac{16z^4}{(x_E - x)^2}. \quad (\text{A23})$$

In binary collisions, the “struck” electron is promoted to a state above the Fermi level; we consider the “primary” electron as the most energetic after the interaction. Recalling that low- W binary collisions occur preferentially with target electrons near the Fermi level, the final energies of the two electrons are equal when $W \sim (E - E_F)/2$. Consequently, we shall assume that the maximum allowed energy loss in binary collisions is $(E - E_F)/2$. Thus, for electrons we take

$$x_{\max}^{(-)} = (x_E - 1)/2. \quad (\text{A24})$$

Integration of the DCS over kinematically allowed recoil energies gives the one-electron energy-loss DCS,

$$\frac{d\sigma_{\text{feg}}}{dx} \equiv \int_{z_-}^{z_+} \frac{d^2\sigma_{\text{feg}}}{dx dz} dz = \frac{2\pi e^4}{EE_F} \int_{z_-}^{z_+} \frac{1}{xz} \frac{df_L(z,x)}{dx} F_{\text{ex}}(z,x) dz, \quad (\text{A25})$$

with [see Eq. (A3)]

$$z_{\pm} = \frac{1}{2}(\sqrt{x_E} \pm \sqrt{x_E - x}). \quad (\text{A26})$$

For positrons, and also for plasmon excitation, the exchange correction factor F_{ex} must be omitted.

The contribution from binary collisions to the energy-loss DCS is

$$\frac{d\sigma_{\text{bc}}}{dx} = \frac{2\pi e^4}{EE_F} \int_{z_-}^{z_+} \frac{6}{16\pi\chi^2} \frac{z\chi^2 f_2(z,x)}{[z^2 + \chi^2 f_1(z,x)]^2 + \chi^4 f_2^2(z,x)} \times F_{\text{ex}}(z,x) dz, \quad (\text{A27})$$

and can be calculated by a single numerical integration. For energy losses much larger than the plasmon-cutoff energy W_c , the finite width of the Lindhard continuum has a negligible effect and the DCS for binary collisions can be closely approximated as

$$\frac{d^2\sigma_{\text{bc}}}{dx dz} = \frac{2\pi e^4}{EE_F} \frac{1}{xz} \delta(x - 4z^2) = \frac{\pi e^4}{EE_F} \frac{1}{x^2} \delta[z - (x^{1/2}/2)]. \quad (\text{A28})$$

With this approximation, we have

$$\frac{d\sigma_{\text{bc}}}{dx} = \frac{\pi e^4}{EE_F} \frac{1}{x^2} \quad (\text{A29})$$

for positrons and

$$\frac{d\sigma_{\text{bc}}}{dx} = \frac{\pi e^4}{EE_F} \frac{1}{x^2} \left[1 - \frac{x}{x_E - x} + \frac{x^2}{(x_E - x)^2} \right] \quad (\text{A30})$$

for electrons. These expressions coincide with the familiar nonrelativistic Rutherford and Møller formulas, which are the correct results for collisions of positrons and electrons with free electrons at rest, within the first Born approximation.

We wish to calculate the total one-electron cross section $\sigma_{\text{bc}}(E, \rho, \Delta)$ for binary collisions with energy transfers W larger than the gap energy Δ , which is

$$\sigma_{\text{bc}}(E, \rho, \Delta) = \int_{\Delta/E_F}^{x_{\text{max}}} \frac{d\sigma_{\text{bc}}}{dx} dx. \quad (\text{A31})$$

To compute the integral in Eq. (A25) over the Lindhard continuum we use an adaptive 20-point Gauss-Legendre algorithm, which delivers results accurate to the order of six significant digits. The integrand in Eq. (A31) is tabulated for a grid of x values suitably spaced to allow accurate log-log interpolation, and the integral of the interpolating function is evaluated analytically.

-
- [1] A. Jablonski and C.J. Powell, *Surf. Sci.* **463**, 29 (2000).
[2] J.M. Fernández-Varea, D. Liljequist, S. Csillag, R. Rätty, and F. Salvat, *Nucl. Instrum. Methods Phys. Res. B* **108**, 35 (1996).
[3] N. F. Mott and H. S. W. Massey, *The Theory of Atomic Collisions* (Oxford University Press, London, 1965).
[4] B.H. Bransden, M.R.C. McDowell, C.J. Noble, and T. Scott, *J. Phys. B* **9**, 1301 (1976).
[5] F. Salvat and R. Mayol, *Comput. Phys. Commun.* **74**, 358 (1993).
[6] J.B. Furness and I.E. McCarthy, *J. Phys. B* **6**, 2280 (1973).
[7] R. Vanderpoorten, *J. Phys. B* **8**, 926 (1975).
[8] C.J. Joachain, R. Vanderpoorten, K.H. Winters, and F.W. Byron, Jr, *J. Phys. B* **10**, 227 (1977).
[9] F.W. Byron, Jr and C.J. Joachain, *Phys. Rep.* **34**, 233 (1977).
[10] I.E. McCarthy, C.J. Noble, B.A. Phillips, and A.D. Turnbull, *Phys. Rev. A* **15**, 2173 (1977).
[11] G. Staszewska, D.W. Schwenke, D. Thirumalai, and D.G. Truhlar, *Phys. Rev. A* **28**, 2740 (1983).
[12] G. Staszewska, D.W. Schwenke, and D.G. Truhlar, *Phys. Rev. A* **29**, 3078 (1984).
[13] I. Bray, D.H. Madison, and I.E. McCarthy, *Phys. Rev. A* **41**, 5916 (1990).
[14] I. Bray, D.A. Kononov, and I.E. McCarthy, *Phys. Rev. A* **44**, 7830 (1991).
[15] I. Bray and D.V. Fursa, *Phys. Rev. Lett.* **76**, 2674 (1996).
[16] D.D. Reid and J.M. Wadehra, *J. Phys. B* **29**, L127 (1996).
[17] J.K. O'Connell and N.F. Lane, *Phys. Rev. A* **27**, 1893 (1983).
[18] N.T. Padial and D.W. Norcross, *Phys. Rev. A* **29**, 1742 (1984).
[19] A. Jain, *Phys. Rev. A* **41**, 2437 (1990).
[20] J. Lindhard, K. Dan. Vidensk. Selsk. Mat. Fys. Medd. **28**, 1 (1954).
[21] V.I. Ochkur, *Zh. Eksp. Teor. Fiz.* **45**, 734 (1963) [*Sov. Phys. JETP* **18**, 503 (1964)].
[22] V.I. Ochkur, *Zh. Eksp. Teor. Fiz.* **47**, 1746 (1964) [*Sov. Phys. JETP* **20**, 1175 (1965)].
[23] B. H. Bransden, *Atomic Collision Theory*, 2nd ed. (Benjamin/Cummings, London, 1983).
[24] J.P. Desclaux, *Comput. Phys. Commun.* **9**, 31 (1975); **13**, 71(E) (1977).
[25] M.E. Riley and D.G. Truhlar, *J. Chem. Phys.* **63**, 2182 (1975).
[26] D. R. Lide, *CRC Handbook of Chemistry and Physics*, 79th ed. (CRC Press, Boca Raton, FL, 1999).
[27] M.H. Mittleman and K.M. Watson, *Ann. Phys. (N.Y.)* **10**, 268 (1960).
[28] S. Seltzer (private communication).
[29] J.P. Perdew and A. Zunger, *Phys. Rev. B* **23**, 5048 (1981).
[30] L.I. Schiff, *Quantum Mechanics* (McGraw-Hill, Tokyo, 1968), p. 130.
[31] D.W. Walker, *Adv. Phys.* **20**, 257 (1971).
[32] M.E. Rose, *Relativistic Electron Theory* (Wiley, New York, 1961).
[33] F. Salvat, J.M. Fernández-Varea, and W. Williamson, *Comput.*

- Phys. Commun. **90**, 151 (1995).
- [34] J. Kessler, Rev. Mod. Phys. **41**, 3 (1969).
- [35] J. Kessler, *Polarized electrons* (Springer-Verlag, Berlin, 1976).
- [36] See http://physics.nist.gov/cgi-bin/AtData/main_asd
- [37] S.C. Gupta and J.A. Rees, J. Phys. B **8**, 1267 (1975).
- [38] R.H.J. Jansen, F.J. de Heer, H.J. Luyken, B. van Wingerden, and H.J. Blaauw, J. Phys. B **9**, 185 (1976).
- [39] J.P. Bromberg, J. Chem. Phys. **61**, 963 (1974).
- [40] J.F. Williams and B.A. Willis, J. Phys. B **8**, 1670 (1975).
- [41] R.D. DuBois and M.E. Rudd, J. Phys. B **9**, 2657 (1976).
- [42] R.W. Wagenaar, A. de Boer, T. van Tubergen, J. Los, and F.J. de Heer, J. Phys. B **19**, 3121 (1986).
- [43] S.C. Gupta and J.A. Rees, J. Phys. B **8**, 417 (1975).
- [44] R. Panajotovic, D. Filipovic, B. Marinkovic, V. Pejcev, M. Kurepa, and L. Vuskovic, J. Phys. B **30**, 5877 (1997).
- [45] S.K. Srivastava, H. Tanaka, A. Chutjian, and S. Trajmar, Phys. Rev. A **23**, 2156 (1981).
- [46] D. Cvejanovic and A. Crowe, J. Phys. B **30**, 2873 (1997).
- [47] L. Vuskovic and M.V. Kurepa, J. Phys. B **9**, 837 (1976).
- [48] H. Nishimura, T. Matsuda, and A. Danjo, J. Phys. Soc. Jpn. **56**, 70 (1987).
- [49] T. Ester and J. Kessler, J. Phys. B **27**, 4295 (1994).
- [50] R.H.J. Jansen and F.J. de Heer, J. Phys. B **9**, 213 (1976).
- [51] J.F. Williams and A. Crowe, J. Phys. B **10**, 2233 (1975).
- [52] A. Danjo, J. Phys. B **21**, 3759 (1988).
- [53] G. Holtkamp, K. Jost, F.J. Peitzmann, and J. Kessler, J. Phys. B **20**, 4543 (1987).
- [54] R. Panajotovic, V. Pejcev, M. Konstantinovic, D. Filipovic, V. Bocvarski, and B. Marinkovic, J. Phys. B **26**, 1005 (1993).
- [55] J.P. Bromberg, J. Chem. Phys. **51**, 4117 (1969).
- [56] I. Iga, L. Mu-Tao, J.C. Nogueira, and R.S. Barbieri, J. Phys. B **20**, 1095 (1987).
- [57] F.J. de Heer, R. Jansen, and W. van der Kaay, J. Phys. B **12**, 979 (1979).
- [58] L. Dou, W.E. Kauppila, C.K. Kwan, and T.S. Stein, Phys. Rev. Lett. **68**, 2913 (1992).
- [59] K. Schackert, Z. Phys. **213**, 316 (1968).
- [60] M.R. Went, R.P. McEachran, B. Lohmann, and W.R. MacGillwray, J. Phys. B **35**, 4885 (2002).
- [61] A. Dorn, A. Elliott, J. Lower, S.F. Mazevet, R.P. McEachran, I.E. McCarthy, and E. Weigold, J. Phys. B **31**, 547 (1998).
- [62] H. Müller and J. Kessler, J. Phys. B **27**, 5893 (1994).
- [63] O. Berger and J. Kessler, J. Phys. B **19**, 3539 (1986).
- [64] M. Inokuti, Rev. Mod. Phys. **43**, 297 (1971).
- [65] R.H. Ritchie, Phys. Rev. **114**, 644 (1959).